e-ISSN: 2805-5756

PENERBIT PRESS
UNIVERSITI TEKNOLOGI MARA

Available online at
https:// jaeds.uitm.edu.my

Journal of Applied Engineering Design and Simulation 6(2) 2026, 146-160

Journal of Applied Engineering Design and Simulation

Effect of excitation frequency and pneumatic pressure on the voltage response of a chemically unmodified chicken feather-based contact-separation triboelectric nanogenerator

Mohd Amirul Ramlan[1], Muhammad Irsyad Missnan[2] , Oskar Hasdinor Hassan[3,4], Panu Thainiramit[5*], Noor Haida Mohd Kaus[6], Muhammad Azhan Anuar[1], Muhammad Aman Haikal[2], Tunku Ishak Tunku Kudin[7,8]

[1]*Faculty of Mechanical Engineering, Universiti Teknologi MARA, 40450, Shah Alam, Selangor Malaysia*
[2]*Faculty of Applied Sciences, Universiti Teknologi MARA, 40450, Shah Alam, Selangor Malaysia*
[3]*College of Creative Arts, Universiti Teknologi MARA, 40450, Shah Alam, Selangor Malaysia*
[4]*Ionics Materials & Devices (iMADE) Research Laboratory, Institute of Science (IOS), Universiti Teknologi MARA, 40450, Shah Alam, Selangor Malaysia*
[5]*Division of Physical Science (Physics), Faculty of Science, Prince of Songkhla University, Songkhla, Thailand*
[6]*School of Chemical Sciences, Universiti Sains Malaysia, 11800, Penang, Malaysia*
[7]*Renewable Energy Program PETRONAS Group Research & Technology, 43000 Bandar Baru Bangi, Selangor, Malaysia*
[8]*Faculty of Defence Science and Technology, Universiti Pertahanan Nasional Malaysia (UPNM)*

ARTICLE INFO

Article history:
Received 6 August 2026
Revised 30 September 2026
Accepted 6 October 206
Online first 15 October 2026
Published 15 October 2026

ABSTRACT

Chemically unmodified waste chicken feathers (CF) offer a potential route for valorising poultry waste as a triboelectric material while avoiding deliberate chemical functionalisation. This study investigates the voltage response of a CF–PTFE contact–separation triboelectric nanogenerator (CS-TENG) under controlled variations in excitation frequency, pneumatic pressure, and CF layer configuration. A full-

[5*]Corresponding author. *E-mail address*: panu.t@psu.ac.th

Keywords:
Triboelectric nanogenerator
Chicken feather waste
Bio-based triboelectric materials
Pneumatic pressure
Contact-Separation mode
Excitation frequency

DOI:

10.24191/jaeds.v6i2.219

factorial combination of three excitation frequencies (0.5, 2.7, and 5.0 Hz), three pneumatic pressures (0.2, 0.4, and 0.6 MPa), and three CF configurations (1CF, 3CF, and 5CF) was evaluated, with each condition tested in three separate experimental runs. Within the investigated ranges, the mean peak-to-peak voltage (Vpp) increased consistently with excitation frequency and pneumatic pressure across all CF configurations. The 3CF configuration produced the highest mean Vpp among the tested configurations, reaching 60.33 ± 0.58 V at 5.0 Hz and 0.6 MPa. These findings establish the experimentally observed voltage response of chemically unmodified waste CF in a CS-TENG and demonstrate systematic variations in response with excitation frequency, pneumatic pressure, and CF layer configuration within the investigated ranges. The results are limited to voltage measurements within these parameter ranges; therefore, further current, charge, load-dependent power, and extended-range measurements are required to establish broader energy-harvesting performance.

Abbreviations

CF	Chicken feather
CS-TENG	Contact-Separation Triboelectric Nanogenerator
EDX	Energy-Dispersive X-ray Spectroscopy
FTIR	Fourier Transform Infrared Spectroscopy
Hz	Hertz
PTFE	Polytetrafluoroethylene
MPa	Megapascal
SEM	Scanning Electron Microscope
Vpp	Peak-to-peak voltage

1. INTRODUCTION

The growing use of portable electronics, wearable devices, wireless sensor networks, and Internet of Things (IoT) technologies has increased interest in energy-harvesting approaches capable of converting ambient mechanical energy into electrical energy [1]. Although conventional batteries remain widely used for powering such systems, their eventual replacement and end-of-life management have motivated research into alternative and complementary power sources [2]. Triboelectric nanogenerators (TENGs) have attracted considerable attention as a means of converting mechanical excitation into electrical output through contact electrification and electrostatic induction [3]. Their relatively simple architecture and compatibility with diverse forms of mechanical excitation have supported their development for energy-harvesting and self-powered sensing applications [1].

Among the fundamental operating modes of triboelectric nanogenerators, the contact–separation (CS) mode provides a relatively simple configuration for converting cyclic mechanical motion into electrical output [4]. In a contact–separation TENG (CS-TENG), electrical output arises from contact electrification between two dissimilar triboelectric materials and the subsequent electrostatic induction associated with their relative separation [3]. The resulting electrical response is therefore closely related to the contact–

separation behaviour of the triboelectric interface, making the mechanical operating conditions an important consideration in CS-TENG performance [5].

The electrical response of contact–separation TENGs can be influenced by mechanical operating conditions, including excitation frequency and interfacial loading [6]. Changes in excitation frequency alter the temporal characteristics of the contact–separation process and have been reported to produce frequency-dependent variations in TENG output [7]. Mechanical loading can likewise influence the electrical response by modifying the contact conditions at the triboelectric interface; in particular, pressure-dependent changes in real contact area and output voltage have been experimentally reported in contact–separation TENG systems [8]. These findings indicate that excitation frequency and mechanical loading are relevant operating parameters when evaluating the electrical response of a CS-TENG.

In parallel with advances in TENG performance, nature-derived and waste-derived materials have attracted increasing interest as alternatives to conventional synthetic triboelectric materials [9]. Chicken feathers are an abundant poultry-industry by-product composed predominantly of keratin and possess a hierarchical structure comprising barbs and barbules [10-11]. Their keratin-rich composition and naturally structured surface have motivated their investigation for triboelectric applications [12], while their use also provides a potential route for value-added utilisation of poultry waste [13]. Previous studies have employed feather structures in single-electrode and rotational TENGs, including surface-modified configurations [14, 15], and processed keratin-rich materials as additives or composites in contact–separation TENGs [16-17]. Chemically unmodified chicken-feather fibres have also been employed in piezoelectric energy harvesters [18]. However, systematic evaluation of chemically unmodified waste chicken feathers as the contact layer of a contact–separation TENG under controlled variations in excitation frequency, pneumatic pressure, and CF layer configuration remains limited.

Accordingly, this study investigates the voltage response of a contact–separation triboelectric nanogenerator incorporating chemically unmodified waste chicken feathers (CF) and PTFE as the opposing triboelectric materials. The prepared CF was characterised using FTIR, SEM, and EDX, while the electrical investigation evaluated the effects of excitation frequency, applied pneumatic pressure, and CF layer configuration on the peak-to-peak voltage (Vpp) of the fabricated CS-TENG. The study establishes experimentally supported voltage-response trends across the investigated operating conditions and clarifies the specific contribution of chemically unmodified waste CF within a contact–separation TENG configuration.

2. MATERIALS AND METHOD

2.1 Materials

Chemically unmodified waste chicken feathers (CF) were collected from a local poultry processing facility and used as the feather-based triboelectric material. Commercially available chicken feathers were additionally obtained as a comparative material for FTIR characterisation and were not used in the fabrication or electrical evaluation of the CS-TENG. A woven glass-fibre-reinforced polytetrafluoroethylene (PTFE) composite was used as the opposing triboelectric material. Aluminium foil was used as the electrode material, while acrylic plates served as rigid supporting substrates for the contact–separation assembly. Cellulose carriers were used to support and arrange the prepared CF contact layers during fabrication of the CF layer configurations.

2.2 Preparation of chicken feathers

The collected chicken feathers were thoroughly washed with distilled water and subsequently cleaned with ethanol. The cleaned feathers were oven-dried at 60 °C for 24 h to reduce residual moisture. No additional chemical treatment or deliberate surface modification was performed after the cleaning and drying procedures. Following drying, the feather barbs, together with their naturally attached barbules, were manually separated from the rachis and arranged adjacent to one another on a cellulose adhesive carrier. The basal ends of the barbs were secured to the cellulose carrier, leaving the barb and barbule structures exposed to form the CF contact surface. The prepared CF material was therefore described as chemically unmodified because no deliberate chemical functionalisation or surface modification was applied.

2.3 Experimental platform

A laboratory-scale pneumatic platform was used to generate controlled vertical contact–separation motion during electrical performance evaluation. The platform consisted of a custom pneumatic actuator positioned vertically above the CS-TENG assembly and mechanically coupled to the upper acrylic support through a 3-mm-diameter connecting rod. The upper assembly formed the moving component of the system, whereas the lower assembly remained stationary during cyclic operation. The actuator had a maximum stroke of 20 mm, while the maximum separation distance used between the opposing triboelectric surfaces was fixed at 13 mm throughout the experiments.

The supporting structure constrained the actuator motion to the vertical direction and maintained alignment between the opposing triboelectric surfaces during repeated contact–separation cycles. Mechanical excitation was controlled by the actuator operating frequency and supplied pneumatic pressure. The actuator operating frequency and pneumatic supply pressure therefore represented the controlled mechanical input parameters of the experimental platform. The normal contact force at the triboelectric interface was not directly measured.

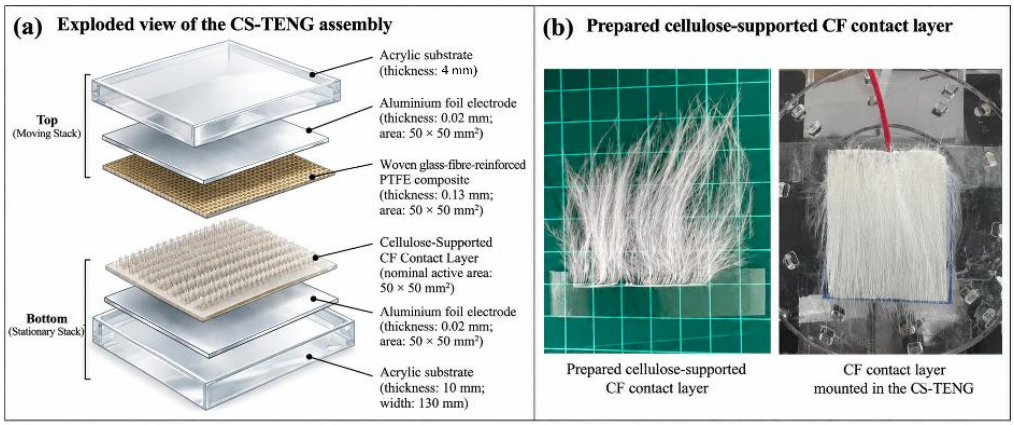


Fig. 1 Configuration and fabrication of the CS-TENG: (a) exploded schematic of the moving upper and stationary lower stacks; and (b) photographs of the prepared cellulose-supported CF contact layer and its placement in the device.

2.4 Fabrication of the CS-TENG

A laboratory-scale pneumatic platform was used to generate controlled vertical contact–separation motion of the CS-TENG. A custom pneumatic actuator was positioned vertically above the device and coupled to the moving upper stack through a 3-mm-diameter connecting rod. The moving stack comprised a 4-mm-thick acrylic support, a 50 × 50 mm² aluminium foil electrode with a thickness of 0.02 mm, and a 0.13-mm-thick woven glass-fibre-reinforced PTFE composite forming the upper triboelectric surface. The actuator had a maximum stroke of 20 mm, while the maximum separation between the opposing triboelectric surfaces was fixed at 13 mm throughout the experiments. The experimental platform is shown in Fig. 2.

The stationary lower stack comprised CF barbs with naturally attached barbules secured at their basal ends to a cellulose adhesive carrier, followed by a 50 × 50 mm² aluminium foil electrode with a thickness of 0.02 mm and a 130-mm-wide, 10-mm-thick acrylic support. Each cellulose-supported CF layer had a total mass of approximately 0.07 g, representing the combined mass of the CF material and cellulose carrier rather than the CF mass loading. The 1CF, 3CF, and 5CF configurations consisted of one, three, and five separately prepared cellulose-supported CF layers, respectively, while the nominal active area was maintained at 50 × 50 mm² for all configurations. During operation, the exposed PTFE and CF surfaces formed the triboelectric interface and underwent repeated vertical contact and separation under pneumatic actuation.

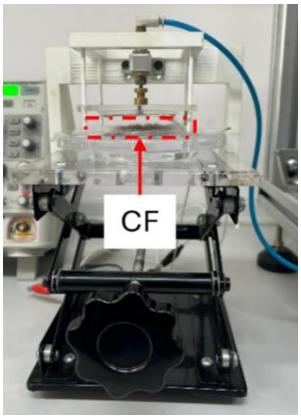


Fig. 2 Laboratory-scale pneumatic experimental platform used to generate vertical contact–separation motion of the CS-TENG.

2.5 Material characterisation

The prepared chicken feathers were characterised using Fourier Transform Infrared Spectroscopy (FTIR), Scanning Electron Microscopy (SEM), and Energy-Dispersive X-ray Spectroscopy (EDX). FTIR analysis of the prepared CF was performed using a PerkinElmer System 2000 over a spectral range of 4000–400 cm^{-1} to identify the principal functional groups associated with the keratin structure. A commercially obtained CF sample was separately characterised using a Shimadzu IRSpirit FTIR spectrometer at a resolution of 8 cm^{-1} with 20 scans. The commercial CF spectrum was used as a comparative reference for the positions of the principal keratin-associated absorption bands. Because the prepared and commercial

CF spectra were acquired using different FTIR instruments, the comparison was limited to the occurrence and approximate positions of the principal absorption bands rather than their relative intensities.

The surface morphology and hierarchical structure of the prepared CF were examined using a Hitachi TM4000Plus benchtop SEM operated at 15 kV with a backscattered-electron detector and a field of view of approximately 107 μm. Elemental composition was analysed using EDX coupled to a JEOL JSM-7600F field-emission scanning electron microscope (FESEM). These analyses were used to characterise the functional groups, surface morphology, and elemental composition of the CF material used in the CS-TENG.

2.6 Electrical response measurement

The electrical response of the fabricated CS-TENG was measured using a Keysight DSOX3014T digital oscilloscope connected to the device electrodes through a Keysight N2843A 10:1 passive probe. The probe provided an input resistance of 10 MΩ when terminated into the 1 MΩ oscilloscope input. The oscilloscope was operated in normal real-time acquisition mode with DC coupling and a 20 MHz bandwidth limit. A horizontal time base of 1.0 s/div was used, and the same measurement configuration was maintained throughout the experimental investigation.

The electrical response was evaluated in terms of the peak-to-peak voltage (Vpp) obtained from the recorded contact–separation waveforms. The exported waveform data contained a temporal interval of 0.005 s between successive data points, corresponding to an effective sampling rate of 200 Sa/s for the exported dataset. Each experimental condition was evaluated in three separate experimental runs (n = 3). Following each run, the actuation was stopped, and the CF contact layer was manually repositioned to restore its arrangement before the subsequent run. The Vpp values obtained from the three runs were used to calculate the mean and sample standard deviation, and the electrical response is therefore reported as mean ± standard deviation.

2.7 Experimental investigation

The experimental investigation was structured to evaluate the electrical response of the CS-TENG across combinations of excitation frequency, applied pneumatic pressure, and CF layer configuration. Preliminary exploratory testing was conducted over an excitation-frequency range of 0.5–5.0 Hz to establish representative operating conditions for the subsequent investigation. Based on this exploratory range, excitation frequencies of 0.5, 2.7, and 5.0 Hz were selected to represent lower, intermediate and upper operating conditions, respectively. This three-level approach was adopted to provide coverage of the investigated frequency range while maintaining a practical number of experimental combinations.

Three levels of applied pneumatic pressure (0.2, 0.4, and 0.6 MPa) and three CF layer configurations (1CF, 3CF, and 5CF) were investigated. The CF configurations corresponded to one, three, and five separately prepared cellulose-supported CF layers, respectively, as described in Section 2.4. All combinations of the three experimental parameters were evaluated, resulting in 27 experimental conditions. Each condition was evaluated in three separate experimental runs, resulting in a total of 81 experimental runs. The maximum separation distance between the opposing triboelectric surfaces was maintained at 13 mm throughout the investigation to provide a consistent contact–separation geometry for comparison of the electrical responses. The selected parameter levels were used to examine performance trends within the investigated operating range rather than to establish a global optimum operating condition.

3. RESULTS AND DISCUSSION

3.1 FTIR analysis

The FTIR spectra of the prepared chemically unmodified CF and the commercially obtained CF are shown in Fig. 3. The prepared CF spectrum exhibited absorption bands at 3270.13, 2928.24, 1626.65, 1529.44, 1449.83, 1236.63, and 1071.66 cm^{-1}. The broad band at 3270.13 cm^{-1} is associated with overlapping O–H and N–H stretching vibrations, while the band at 2928.24 cm^{-1} is attributable to aliphatic C–H stretching. The prominent bands at 1626.65, 1529.44, and 1236.63 cm^{-1} occurred within the characteristic Amide I, Amide II, and Amide III regions, respectively. These absorption regions are consistent with FTIR characteristics previously reported for chicken-feather keratin [19, 20] and with the proteinaceous keratin structure of avian feathers [10, 21]. For comparison, the commercially obtained CF exhibited corresponding major absorption bands at 3271.03, 1622.59, 1524.95, 1447.41, and 1232.02 cm^{-1}. The close correspondence in the positions of these principal bands indicates that both feather samples exhibited similar keratin-associated spectral features. Because the two spectra were acquired using different FTIR instruments, the comparison was restricted to the occurrence and approximate positions of the principal absorption bands rather than their relative intensities or peak areas.

The FTIR results therefore establish the presence of the principal keratin-associated functional groups in the prepared CF used in the CS-TENG. Surface chemistry and functional groups are known to influence charge generation during contact electrification [5, 22]. However, the present FTIR measurements do not establish the individual contribution of these functional groups to charge transfer at the CF–PTFE interface. Furthermore, because a pre-cleaning FTIR spectrum of the collected CF was not available, the results cannot determine whether the washing, ethanol-cleaning, and drying procedures preserved or altered the original surface chemistry. Accordingly, the FTIR results characterise the chemical functionalities present in the prepared, chemically unmodified CF rather than demonstrate preservation of its original chemical state.

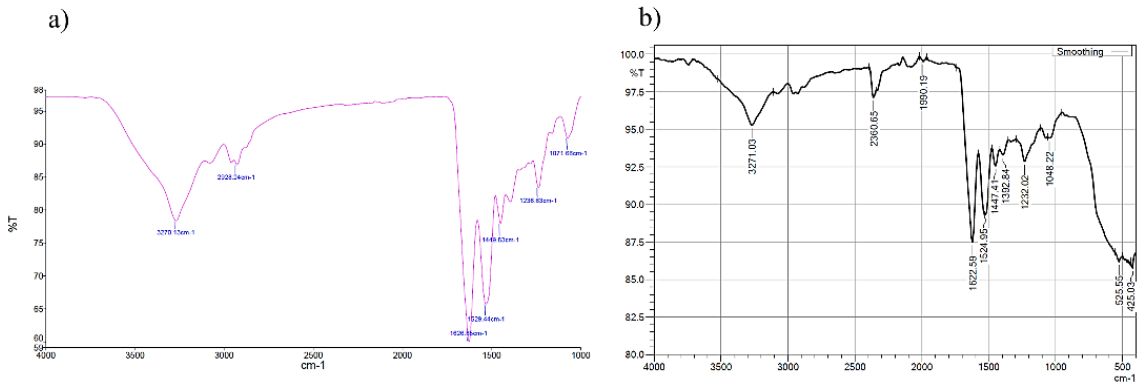


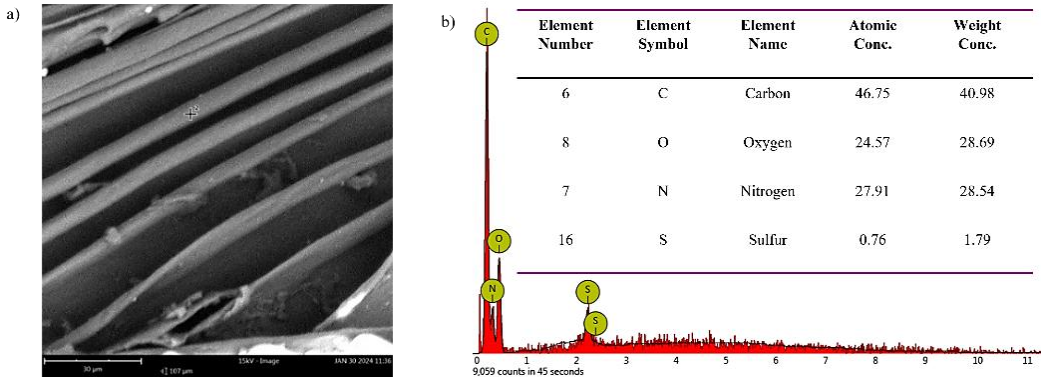
Fig. 3 FTIR spectra of (a) prepared chemically unmodified CF and (b) commercial CF, showing the principal keratin-associated bands.

3.2 SEM and EDX analysis

The surface morphology and elemental composition of the prepared chemically unmodified CF were examined using SEM and EDX, respectively, as shown in Fig. 4. The SEM micrograph in Fig. 4(a), acquired at a field of view of approximately 107 µm, shows the elongated fibrous morphology of the prepared feather material, with longitudinal surface features and microscale surface irregularities visible along the feather structures. These observations demonstrate that the CF contact material possesses a naturally structured, non-planar surface rather than a smooth continuous surface.

The EDX analysis in Fig. 4(b) detected carbon (C), oxygen (O), nitrogen (N), and sulfur (S), with atomic concentrations of 46.75%, 24.57%, 27.91%, and 0.76%, respectively. These elements are consistent with the elemental constituents expected for keratin-based feather material [10, 21]. In particular, the detection of sulfur is consistent with the presence of sulfur-containing amino-acid residues associated with keratin structure [10, 21]. However, EDX provides elemental rather than molecular or bonding information; therefore, the detected sulfur cannot independently establish the presence or configuration of specific sulfur-containing bonds.

The SEM and EDX results therefore characterise the surface morphology and elemental composition of the prepared CF used in the CS-TENG. Surface morphology can influence the interfacial contact conditions involved in contact electrification [5, 9], while keratin-based biowaste materials have been reported as triboelectrically active materials [9, 22]. Nevertheless, the present SEM image does not directly quantify the real contact area at the CF–PTFE interface, and the EDX measurement does not establish the individual contribution of the detected elements to charge transfer. Furthermore, because corresponding SEM and EDX measurements of the CF before cleaning were not available, these results cannot determine whether the preparation procedure preserved or altered the original surface morphology or elemental composition. The analyses were therefore interpreted as characterisation of the prepared CF rather than evidence of morphological or compositional preservation during cleaning.



Element Number	Element Symbol	Element Name	Atomic Conc.	Weight Conc.
6	C	Carbon	46.75	40.98
8	O	Oxygen	24.57	28.69
7	N	Nitrogen	27.91	28.54
16	S	Sulfur	0.76	1.79

Fig. 4 SEM and EDX characterisation of the prepared chemically unmodified CF: (a) surface morphology and (b) elemental composition

3.3 Effect of excitation frequency on voltage

The effect of excitation frequency on the electrical response of the CS-TENG was investigated at 0.5, 2.7, and 5.0 Hz. These frequencies represent the lower, intermediate, and upper conditions selected from the preliminary operating range of 0.5–5.0 Hz, as described in Section 2.7. Fig. 5(a) presents representative output-voltage waveforms obtained at the three excitation frequencies, while Fig. 5(b) compares the corresponding mean peak-to-peak voltage (Vpp) for the 1CF, 3CF, and 5CF configurations at a pneumatic pressure of 0.6 MPa.

Within the investigated frequency range, increasing the excitation frequency resulted in a consistent increase in mean Vpp for all three CF configurations at 0.6 MPa. For the 1CF configuration, the mean Vpp increased from 25.33 ± 0.58 V at 0.5 Hz to 32.33 ± 1.15 V at 2.7 Hz and 41.67 ± 0.58 V at 5.0 Hz. The 3CF configuration exhibited a similar trend, increasing from 45.00 ± 1.00 V at 0.5 Hz to 54.67 ± 2.52 V at 2.7 Hz and 60.33 ± 0.58 V at 5.0 Hz. For the 5CF configuration, the corresponding mean Vpp increased from 29.67 ± 0.58 V to 42.67 ± 0.58 V and 49.33 ± 0.58 V, respectively. The highest mean Vpp measured under these conditions was therefore 60.33 ± 0.58 V, obtained at 5.0 Hz using the 3CF configuration.

The consistent increase in Vpp with excitation frequency indicates a frequency-dependent electrical response within the investigated range. Frequency-dependent variations in TENG output have previously been associated with changes in the mechanical and interfacial conditions of triboelectric operation [7]. Kumar et al. [8] specifically reported an increase in peak-to-peak output voltage with increasing oscillation frequency in a contact–separation TENG, although the materials and operating conditions differed from those used in the present study. More generally, interfacial contact conditions are recognised as important factors governing TENG output [5], while charge-density behaviour represents another important consideration in triboelectric energy generation [23].

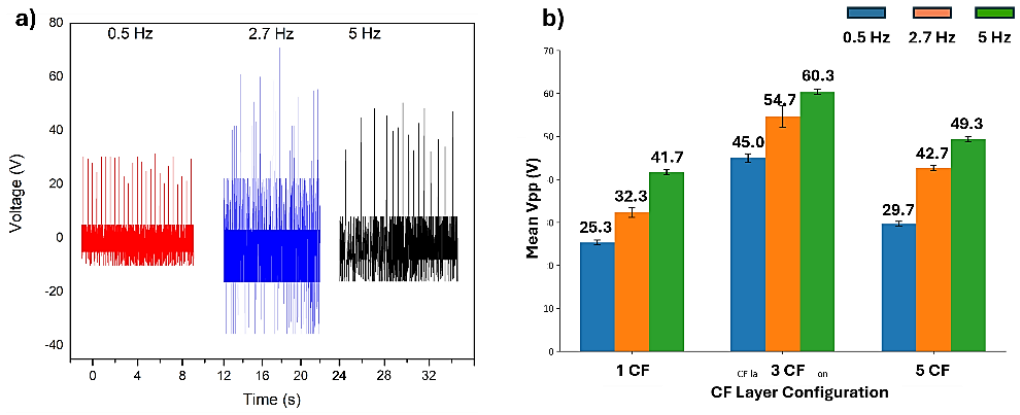


Fig. 5 Effect of excitation frequency on the electrical response of the CS-TENG: (a) representative output-voltage waveforms at 0.5, 2.7, and 5.0 Hz and (b) mean peak-to-peak voltage (Vpp) for the 1CF, 3CF, and 5CF configurations at 0.6 MPa.

Nevertheless, the increase in Vpp observed in the present study should not be attributed solely to the greater number of contact–separation cycles occurring per unit time because Vpp represents the amplitude of the measured voltage waveform rather than cumulative electrical output. Changes in excitation frequency may also modify the dynamic contact–separation conditions of the triboelectric interface [8]. Interfacial contact conditions can influence triboelectric output [5], while the resulting electrical response is also dependent on charge-generation and charge-retention behaviour [23]. However, contact and separation velocity, contact duration, surface charge, and transferred charge were not independently measured in the present study. Therefore, the present voltage measurements alone cannot quantitatively resolve the individual mechanisms responsible for the observed frequency-dependent increase in Vpp.

Overall, the results demonstrate that Vpp increased with excitation frequency over the investigated range of 0.5–5.0 Hz. Among the three frequencies tested, 5.0 Hz produced the highest mean Vpp. Because 5.0 Hz represents the upper boundary of the investigated frequency range, this result does not establish 5.0 Hz as the optimum excitation frequency of the CS-TENG. To determine whether the voltage response continues to increase or reaches a maximum at a higher excitation frequency, measurements beyond 5.0 Hz, together with direct characterisation of the contact–separation kinematics and charge-transfer behaviour, are required.

3.4 Effect of pneumatic pressure on voltage response

Fig. 6 compares the mean peak-to-peak voltage (Vpp) of the 1CF, 3CF, and 5CF configurations at pneumatic pressures of 0.2, 0.4, and 0.6 MPa and excitation frequencies of 0.5, 2.7, and 5.0 Hz. Error bars represent the sample standard deviation of three separate experimental runs (n = 3). Mean Vpp increased with pneumatic pressure at every fixed combination of excitation frequency and CF layer configuration. At 5.0 Hz, increasing the pneumatic pressure from 0.2 to 0.6 MPa increased the mean Vpp from 33.33 ± 1.53 to 41.67 ± 0.58 V for 1CF, from 46.67 ± 1.53 to 60.33 ± 0.58 V for 3CF, and from 37.00 ± 2.65 to 49.33 ± 0.58 V for 5CF. The highest mean Vpp within the experimental matrix was 60.33 ± 0.58 V at 0.6 MPa and 5.0 Hz using 3CF. Complete mean Vpp values and sample standard deviations for all investigated conditions are summarised in Table 1.

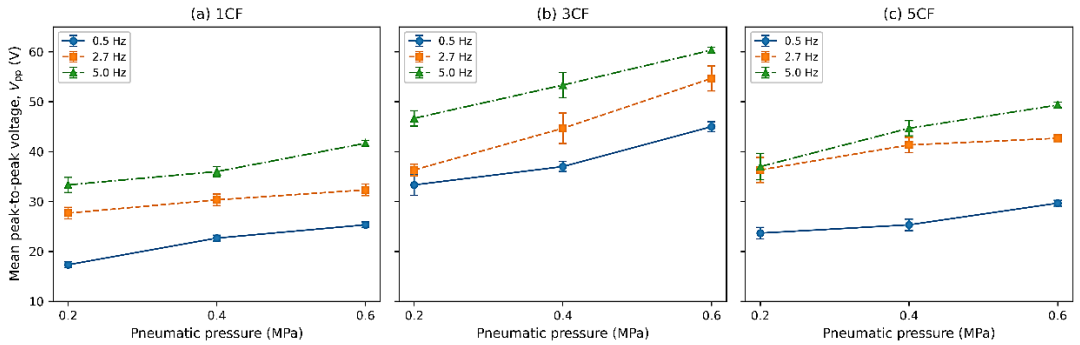


Fig. 6 Mean peak-to-peak voltage (Vpp) as a function of pneumatic pressure for (a) 1CF, (b) 3CF, and (c) 5CF configurations

As summarised in Table 1, the pressure-dependent increase in mean Vpp was observed not only at 5.0 Hz but also at 0.5 and 2.7 Hz for all three CF layer configurations. The magnitude of the increase, however, varied across the investigated frequency and CF layer combinations. Pressure- or load-dependent electrical responses have also been reported for other keratinous-material TENG interfaces. For example, Ali et al. [24] observed an increase in generated voltage when the normal load applied to a rabbit-fur/PTFE contact–separation interface was increased from 3.3 to 20.5 N. Kumar et al. [8] likewise reported pressure-dependent changes in TENG output associated with variations in real contact area at the triboelectric interface. However, direct quantitative comparison with the present experiment is not appropriate because these studies controlled mechanical loading differently, whereas the present platform controlled pneumatic supply pressure and did not directly measure the resulting normal contact force.

In the present experiment, pneumatic supply pressure was the controlled mechanical input parameter, whereas the normal contact force at the CF–PTFE interface was not directly measured. The real contact area, deformation of the CF layers, interfacial pressure distribution, and transferred charge were also not independently measured. Although changes in interfacial contact conditions provide a plausible interpretation of the observed pressure-dependent voltage response [8], the individual mechanisms responsible for the increase in Vpp cannot be determined from the present measurements alone. To further position the present voltage response within the broader literature, Table 2 compares representative feather-, keratin-, and poultry-biowaste-based TENG studies in terms of material treatment, operating mode, excitation conditions, and reported electrical output.

The comparison shows that reported electrical outputs vary substantially across the literature because of differences in biological material, material processing, device architecture, mechanical excitation, and voltage metric. Accordingly, the values in Table 2 should not be interpreted as a direct performance ranking. The present study is distinguished by its controlled and replicated evaluation of chemically unmodified waste chicken-feather layers in a CF–PTFE contact–separation configuration under systematic variations in excitation frequency, pneumatic pressure, and CF layer configuration.

Table 1 Mean peak-to-peak voltage of the CS-TENG under the experimental conditions investigated.

Frequency (Hz)	Pressure (MPa)	1 CF (V)	3 CF (V)	5 CF (V)
0.5	0.2	17.33 ± 0.58	33.33 ± 2.08	23.67 ± 1.15
0.5	0.4	22.67 ± 0.58	37.00 ± 1.00	25.33 ± 1.15
0.5	0.6	25.33 ± 0.58	45.00 ± 1.00	29.67 ± 0.58
2.7	0.2	27.67 ± 1.15	36.33 ± 1.15	36.33 ± 2.52
2.7	0.4	30.33 ± 1.15	44.67 ± 3.06	41.33 ± 1.53
2.7	0.6	32.33 ± 1.15	54.67 ± 2.52	42.67 ± 0.58
5.0	0.2	33.33 ± 1.53	46.67 ± 1.53	37.00 ± 2.65
5.0	0.4	36.00 ± 1.00	53.33 ± 2.52	44.67 ± 1.53
5.0	0.6	41.67 ± 0.58	60.33 ± 0.58	49.33 ± 0.58

Source: Authors' own data

Table 2 Quantitative comparison of representative feather-, keratin-, and poultry-biowaste-based TENGs with the present study

Study	Material/treatment and TENG configuration	Excitation/loading condition	Reported electrical output	Ref.
Zhu et al. (2021)	Natural feather with Cu sputtered as electrode; single-electrode F-STENG	External contact/release; frequency and load not reported	V_{OC} = 90 V; I_{SC} = 3.5 μA	[14]
Cho et al. (2019)	Owl feather with haematoxylin adsorption; Teflon counter surface; rotational wind-driven TENG	Wind speed = 7 m s^{-1}; friction area = 1.6 cm^2	Output voltage = 64.3 V; output current = 6.55 μA	[15]
Singh et al. (2020)	Ethanol-washed and chopped dog hair against PTFE; vertical contact–separation TENG	Manual tapping; force and frequency uncontrolled	$V_{pp} \approx 200$ V	[25]
Joo et al. (2022)	5 wt% human-hair-derived keratin particles incorporated into PVB against PFA; vertical contact–separation TENG	5 N, 5 Hz; active area = 2.5 × 2.5 cm^2	V_{OC} = 296 V; I_{SC} = 37.6 μA; maximum power density ≈ 0.6 mW cm^{-2} at 10 MΩ	[16]
Khan et al. (2023)	Chicken skin against Kapton; contact–separation TENG	4–14 Hz using a linear damping system; force range 1–5 N	$V_{OC} \approx 123$ V and $I_{SC} \approx 20$ μA at 14 Hz; power density = 0.2 mW cm^{-2} at 20 MΩ	[26]
Present study	Chemically unmodified waste CF layers against PTFE; vertical contact–separation CS-TENG	0.5–5.0 Hz; 0.2–0.6 MPa; 13 mm separation	**Mean V_{pp} = 60.33 ± 0.58 V at 5.0 Hz, 0.6 MPa, 3CF (n = 3)**	This study

Source: Compiled from the cited literature and authors' own experimental data

Overall, increasing the applied pneumatic pressure from 0.2 to 0.6 MPa was consistently accompanied by an increase in mean Vpp across all investigated frequency and CF layer combinations. Among the three pressure levels tested, 0.6 MPa produced the highest mean Vpp for each investigated combination. However, because 0.6 MPa was the upper boundary of the investigated pressure range, the present results did not establish 0.6 MPa as the optimum pneumatic pressure of the CS-TENG. Further investigation over an extended pressure range would be required to determine whether the voltage response subsequently reaches a maximum or saturation region.

4. CONCLUSIONS

A contact–separation triboelectric nanogenerator (CS-TENG) incorporating chemically unmodified waste chicken feathers (CF) and PTFE was successfully fabricated and experimentally evaluated. FTIR, SEM, and EDX characterised the keratin-associated functional groups, surface morphology, and elemental composition of the prepared CF. Electrical measurements showed that the mean peak-to-peak voltage (Vpp) increased with excitation frequency from 0.5 to 5.0 Hz and with pneumatic pressure from 0.2 to 0.6 MPa within the investigated ranges. Among the tested CF configurations, 3CF consistently produced the highest mean Vpp. The highest measured response was 60.33 ± 0.58 V, obtained at 5.0 Hz and 0.6 MPa using the 3CF configuration.

These findings demonstrate the voltage response of a chemically unmodified CF–PTFE CS-TENG under controlled variations in excitation frequency, pneumatic pressure, and CF layer configuration. However, the tested ranges did not establish globally optimum operating conditions, and the present electrical evaluation was limited to Vpp measurements. Further investigation incorporating direct contact-force measurements, extended operating ranges, and current, transferred-charge, load-dependent power,

and durability measurements is required to establish the broader energy-harvesting performance and practical applicability of the device.

5. ACKNOWLEDGEMENTS/FUNDING

This research was supported by the PhD. Student Exchange Scholarship from Prince of Songkhla University (PSU) and the Hadiah Latihan Persekutuan (HLP) scholarship from the Ministry of Higher Education (MOHE), Malaysia. Financial support was also provided by PETRONAS Research Sdn. Bhd. (PRSB) under the project "A Rotational Smart Nanogenerator for Efficient Energy Harvesting" (Grant No. UTV/CS/P20220707006). The authors gratefully acknowledge the Division of Physical Science (Physics), Faculty of Science, Prince of Songkhla University, where the experimental work was conducted. Appreciation is also extended to the Faculty of Mechanical Engineering and the Ionics Materials & Devices (iMADE) Research Laboratory, Institute of Science (IOS), Universiti Teknologi MARA (UiTM), as well as the Faculty of Engineering (FKJ), Universiti Pertahanan Nasional Malaysia (UPNM), for their institutional, technical, and laboratory support.

6. CONFLICT OF INTEREST STATEMENT

The authors agree that this research was conducted in the absence of any self-benefits, commercial or financial conflicts and declare the absence of conflicting interests with the funders.

7. AUTHORS' CONTRIBUTIONS

Mohd Amirul Ramlan: Conceptualisation, methodology, formal analysis, data curation, original draft preparation**,** data collection and visualisation, interpretation of results, writing - review and editing; **Muhammad Irsyad Missnan**: Methodology, formal analysis, data curation, original draft preparation, writing - review and editing; **Oskar Hasdinor Hassan**: Resources, supervision, writing - review and editing, and validation. **Panu Thainiramit**: Conceptualisation, supervision, resources, methodology, formal analysis, data curation, original draft preparation, writing - review and editing; **Noor Haida Mohd Kaus**: Supervision, resources, writing - review and editing; **Muhammad Azhan Anuar**: Supervision, resources, writing - review and editing; **Muhammad Aman Haikal Razali**: Writing - review and editing. **Tunku Ishak Tunku Kudin**: Data curation and visualisation, writing - review and editing.

8. DECLARATION OF GENERATIVE AI IN THE WRITING PROCESS

During the preparation of this work, the authors used ChatGPT (OpenAI) to ***improve the readability and language quality of the manuscript****. After using this tool/service, the authors reviewed and edited the content as needed and take full responsibility for the content of the publication.*

9. DATA AVAILABILITY/SUPPLEMENTARY MATERIALS

The datasets used and/or analysed during the current study are available from the corresponding author on reasonable request.

10. ETHICS STATEMENT

The authors declare that this research did not involve human participants or live animal subjects. The chicken feathers used in this study were obtained as waste material from a poultry processing facility, and no animals were specifically used or subjected to experimental procedures for this research. All experimental procedures were performed following the institutional Safety, Health, and Environmental (HSE) protocols of Universiti Teknologi MARA.

11. REFERENCES

[1] Z. L. Wang, J. Chen, and L. Lin, "Progress In Triboelectric Nanogenerators As A New Energy Technology and Self-Powered Sensors," *Energy and Environmental Science*, vol. 8, no. 8., pp. 2250–2282, 2015. doi: 10.1039/c5ee01532d.

[2] G. Harper *et al.*, "Recycling Lithium-Ion Batteries From Electric Vehicles," *Nature*, vol. 575, no. 7781., pp. 75–86, Nov. 07, 2019. doi: 10.1038/s41586-019-1682-5.

[3] W. G. Kim, D. W. Kim, I. W. Tcho, J. K. Kim, M. S. Kim, and Y. K. Choi, "Triboelectric Nanogenerator: Structure, Mechanism, and Applications," *ACS Nano*, vol. 15, no. 1., pp. 258–287, Jan. 26, 2021. doi: 10.1021/acsnano.0c09803.

[4] F. R. Fan, Z. Q. Tian, and Z. Lin Wang, "Flexible Triboelectric Generator," *Nano Energy*, vol. 1, no. 2, pp. 328–334, Mar. 2012, doi: 10.1016/J.NANOEN.2012.01.004.

[5] D. W. Kim, J. H. Lee, J. K. Kim, and U. Jeong, "Material Aspects of Triboelectric Energy Generation And Sensors", vol. 12, no. 1. Dec. 01, 2020. doi: 10.1038/s41427-019-0176-0.

[6] K. Xiao, W. Wang, K. Wang, H. Zhang, S. Dong, and J. Li, "Improving Triboelectric Nanogenerators Performance Via Interface Tribological Optimisation: A Review," *Adv. Funct. Mater.*, vol. 34, no. 39, p. 2404744, Sep. 2024, doi: 10.1002/adfm.202404744.

[7] C. Li, Y. Bai, J. Shao, H. Meng, and Z. Li, "Strategies to Improve the Output Performance of Triboelectric Nanogenerators," *Small Methods*, vol. 8, no. 10, p. 2301682, Oct. 2024, doi: 10.1002/smtd.202301682.

[8] C. Kumar *et al.*, "Multiscale In-situ Quantification of The Role of Surface Roughness and Contact Area Using A Novel Mica-PVS Triboelectric Nanogenerator," *Nano Energy*, vol. 107, p. 108122, Mar. 2023, doi: 10.1016/j.nanoen.2022.108122.

[9] K. Y. Song *et al.*, "Recent Progress On Nature-Derived Biomaterials For Eco-friendly Triboelectric Nanogenerators," *EcoMat*, vol. 5, no. 8, pp. 1–27, 2023, doi: 10.1002/eom2.12357.

[10] J. McKittrick, P. Y. Chen, S. G. Bodde, W. Yang, E. E. Novitskaya, and M. A. Meyers, "The Structure, Functions, and Mechanical Properties of Keratin," *JOM*, vol. 64, no. 4, pp. 449–468, 2012, doi: 10.1007/s11837-012-0302-8.

[11] N. Reddy and Y. Yang, "Structure And Properties of Chicken Feather Barbs as Natural Protein Fibres," *J. Polym. Environ.*, vol. 15, no. 2, pp. 81–87, Apr. 2007, doi: 10.1007/s10924-007-0054-7.

[12] Y. Huang, H. Zheng, J. Zhang, Y. Shen, and X. Xu, "Native Proteins For Triboelectric Nanogenerators," *J. Mater. Chem. C*, vol. 13, no. 6, pp. 2578–2605, 2025, doi: 10.1039/D4TC02923B.

[13] H. Dutta *et al.*, "Biopolymer Composites With Waste Chicken Feather Fillers: A Review," *Renew. Sustain. Energy Rev.*, vol. 197, p. 114394, Jun. 2024, doi: 10.1016/J.RSER.2024.114394.

[14] J. Zhu, Y. Cheng, S. Hao, Z. L. Wang, N. Wang, and X. Cao, "A Self-Healing Triboelectric Nanogenerator Based on Feathers for Sensing and Energy Harvesting," *Adv. Funct. Mater.*, vol. 31, no. 34, Aug. 2021, doi: 10.1002/adfm.202100039.

[15] Y. Cho *et al.*, "Rotational Wind Power Triboelectric Nanogenerator Using Aerodynamic Changes of Friction Area And The Adsorption Effect of Hematoxylin Onto Feather Based On A Diversely Evolved Hyper-Branched Structure," *Nano Energy*, vol. 61, pp. 370–380, Jul. 2019, doi: 10.1016/j.nanoen.2019.04.083.

[16] S. Joo *et al.*, "Eco-Friendly Keratin-Based Additives in the Polymer Matrix to Enhance the Output of Triboelectric Nanogenerators," *ACS Appl. Bio Mater.*, vol. 5, no. 12, pp. 5706–5715, 2022, doi: 10.1021/acsabm.2c00736.

[17] K. G. Motora, "Waste-to-Energy: Development of a Highly Efficient Keratin Enhanced Chitosan Bio-Waste-Derived Triboelectric Nanogenerator for Energy Harvesting and Real Applications," *Adv. Funct. Mater.*, vol. 34, no. 22, p. 2315069, 2024, doi: 10.1002/adfm.202315069.

[18] E. Kar *et al.*, "Chicken Feather Fibre-Based Bio-Piezoelectric Energy Harvester: An Efficient Green Energy Source For Flexible Electronics," *Sustain. Energy Fuels*, vol. 5, no. 6, pp. 1857–1866, Mar. 2021, doi: 10.1039/d0se01433h.

[19] X.-C. Yin, F.-Y. Li, Y.-F. He, Y. Wang, and R.-M. Wang, "Study On Effective Extraction of Chicken Feather Keratins and Their Films for Controlling Drug Release," *Biomater. Sci.*, vol. 1, no. 5, pp. 528–536, May 2013, doi: 10.1039/c3bm00158j.

[20] S. Mattiello *et al.*, "Physico-Chemical Characterisation of Keratin from Wool and Chicken Feathers Extracted Using Refined Chemical Methods," *Polymers (Basel).*, vol. 15, no. 1, pp. 1–15, 2023, doi: 10.3390/polym15010181.

[21] B. Wang, W. Yang, J. McKittrick, and M. A. Meyers, "Keratin: Structure, Mechanical Properties, Occurrence in Biological Organisms, and Efforts at Bioinspiration," *Progress in Materials Science*, vol. 76., pp. 229–318, Mar. 01, 2016. doi: 10.1016/j.pmatsci.2015.06.001.

[22] A. Bhaduri and T. J. Ha, "Biowaste-Derived Triboelectric Nanogenerators for Emerging Bioelectronics," *Advanced Science*, vol. 11, no. 42., Nov. 13, 2024. doi: 10.1002/advs.202405666.

[23] X. Cui, J. Nie, and Y. Zhang, "Recent Advances In High Charge Density Triboelectric Nanogenerators," *International Journal of Extreme Manufacturing*, vol. 6, no. 4., Aug. 01, 2024. doi: 10.1088/2631-7990/ad39ba.

[24] A. Al-Kabbany, A. S, and W. Ali, "Voltage Generated From Triboelectrification of Rabbit Fur and Polymeric Materials," *J. Egypt. Soc. Tribol.*, vol. 19, no. 3, pp. 10–18, Jul. 2022, doi: 10.21608/JEST.2022.249530.

[25] M. Singh, A. Sheetal, H. Singh, R. S. Sawhney, and J. Kaur, "Animal Hair-Based Triboelectric Nanogenerator (TENG): A Substitute for the Positive Polymer Layer in TENG," *J. Electron. Mater.*, vol. 49, no. 5, pp. 3409–3416, 2020, doi: 10.1007/s11664-020-08031-y.

[26] M. U. Khan, E. Mohammad, Y. Abbas, M. Rezeq, and B. Mohammad, "Chicken Skin-Based Milli Watt Range Biocompatible Triboelectric Nanogenerator for Biomechanical Energy Harvesting," *Sci. Rep.*, vol. 13, no. 1, Dec. 2023, doi: 10.1038/s41598-023-36817-7.

© 2026 by the authors. Submitted for possible open access publication under the terms and conditions of the Creative Commons Attribution (CC BY-NC-ND) license (http://creativecommons.org/licenses/by/4.0/).